8A.2

Spatial structure of the raindrop size distribution at small scale

Joël Jaffrain* and Alexis Berne

Environmental Remote Sensing Lab. (LTE),
École Polytechnique Fédérale de Lausanne, Switzerland

1 INTRODUCTION

Rainfall is a physical process highly variable in time and space, which makes its quantification difficult especially because of the problem of the spatial representativity (point, volume) of the measurements. While investigations on the spatial variability of the raindrop size distribution (DSD) are becoming more and more common in the recent years (e.g., Lee et al., 2009; Tokay and Bashor, 2010; Tapiador et al., 2010), most of the experimental setups did not allow to fully characterize the spatial variability of the DSD for distance lags below 1 km (which is the typical size of a weather radar pixel). This work investigate the variability of the DSD at the radar subgrid scale ($\sim$1 km^2) based on an experimental approach. Section 2 presents the considered data set and the methods while the quantification of the spatial structure of the DSD is provided in Section 3. Finally, Section 4 draws some conclusions.

2 DATASET AND METHODS

2.1 Experimental setup

A network of 16 optical disdrometers PARSIVEL (OTT) has been deployed over a typical weather radar pixel ($\sim$1$\times$1 km^2) in Lausanne, Switzerland. 16 sampling locations provide a total of 120 pairs of points. According to the configuration of the network, the interdistances between pairs of instruments is ranging from 80 m to about 800 m. The network is presented in details in Jaffrain et al. (2011).

The network has collected DSD spectra at a 30-s temporal resolution for about 16 months. 36 rainfall events have been selected and classified in different types according to visual inspection of radar rainrate maps. 9, 19 and 8 rainfall events have been identified as convective, transitional and frontal respectively. It corresponds to about 643, 3665 and 839 rainy minutes respectively. Statistics characterizing each group of rainfall are presented in Table 1.

* *Corresponding author address:* Joël Jaffrain, LTE, Station 2, EPFL, 1015 Lausanne, Switzerland;
e-mail: joel.jaffrain@epfl.ch

2.2 Methods

Similarly to Jaffrain and Berne (2011), a filtering process is applied on the data prior to the analyses. For consistency and to limit the influence of very weak rainfall, all the stations must record a rain rate higher than 0.1 mm h^{-1}. To filter out possible non natural drops, raindrops outside $\pm$60% around the terminal fall speed-diameter relationship are removed (see Kruger and Krajewski, 2002; Jaffrain and Berne, 2011).

Using a statistical approach, the raindrop size distribution can be seen as the product between the total concentration of drops N_t and a probability density function $f(D)$. A commonly used statistical descriptor to characterize the first order moment of $f(D)$ is the mass-weighted diameter D_m. As a result, information on the variability of these two quantities will provide an estimation of the variability of the DSD. Moreover, analyses have been conducted as well for different quantities related to the DSD but to keep this paper short, only the rain rate R, which is of primary importance for many environmental applications, is presented hereafter.

Because the mean is involved, classical tools to characterize the spatial structure (e.r., autocorrelation, variograms) are well suited for Gaussian-like distributed random fields. Consequently, the logarithm transform of the different quantities is considered as this leads to more symmetrical distributions.

In the following, $V(x)$ is defined as a stationary random function which has a lognormal distribution. Defining $Y(x) = \ln[V(x)]$, the means m_Y and m_V, the variances σ_Y^2 and σ_V^2 and the covariances $C_Y(h)$ and $C_V(h)$ of Y and V are related as follows (Chilès and Delfiner, 1999, p. 103):

$$m_V = \exp\left(m_Y + \frac{1}{2}\sigma_Y^2\right) \quad (1)$$

$$\sigma_V^2 = m_V^2\left[\exp\left(\sigma_Y^2\right) - 1\right] \quad (2)$$

$$C_V(h) = m_V^2\left\{\exp\left[C_Y(h)\right] - 1\right\} \quad (3)$$

where m_Y and σ_Y are the mean and the standard deviation of the population of Y values.

The (semi)variogram is a key tool used in Geostatistics in order to investigate and quantify the

Table 1: Statistics of the three different groups of rainfall events at a 60-s temporal resolution.

	Convective	Transitional	Frontal
Number of events	9	19	8
Number of rainy minutes	643	3665	839
Rain amount averaged over the network [mm]	32.6	113.7	10.5
Mean of the averaged rain rate $\overline{R}$ [mm h^{-1}]	3.05	1.86	0.75
$Q_{10\%}(\overline{R})$ [mm h^{-1}]	0.50	0.33	0.25
$Q_{50\%}(\overline{R})$ [mm h^{-1}]	2.42	1.24	0.64
$Q_{90\%}(\overline{R})$ [mm h^{-1}]	5.98	4.12	1.33

spatial (or temporal) structure of a random function $V(x)$ (Matheron, 1965). It is expressed as:

$$\gamma(h) = \frac{1}{2}\mathrm{E}\left\{[V(x+h) - V(x)]^2\right\} \quad (4)$$

where E denotes the expectation, x is a position vector and h is a distance (or time) separation vector.

The classical widely used sample variogram estimator, sometimes called "Matheron" estimator, is expressed as (Chilès and Delfiner, 1999):

$$\hat{\gamma}(h) = \frac{1}{2N_h}\sum_{x_\beta - x_\alpha \simeq h}\left\{[v(x_\beta) - v(x_\alpha)]^2\right\} \quad (5)$$

where N_h is the number of pairs (x_α,x_β) separated by a distance approximately equal to h. As the mean is involved, the quality of $\hat{\gamma}(h)$ estimates is influenced by the possible skewness of the distribution of the increment values. A more robust estimator based on the quantile variogram $\hat{\gamma}_p(h)$, as defined by Armstrong and Delfiner (1980), can be used:

$$\hat{\gamma}_p(h) = \underset{x_\beta - x_\alpha \simeq h}{Q_p}\left\{\frac{1}{2}[v(x_\beta) - v(x_\alpha)]^2\right\} \quad (6)$$

where Q_p denotes the quantile with a probability $p \in]0,1[$. Quantile variograms are all proportional to the classical variogram with proportionality factors being the quantiles of the distribution of a chi-square variable with one degree freedom χ^2_1 (Chilès and Delfiner, 1999) when V is bi-normal. For robustness, the median variogram estimator is used to estimate the variogram according to:

$$\hat{\gamma}(h) = \frac{\hat{\gamma}_{0.50}(h)}{Q_{0.50}(\chi^2_1)} \quad (7)$$

where $Q_{0.50}(\chi^2_1)$ is the median of a χ^2_1 distribution which is equal to 0.455.

The next step consists in back-transforming into linear space the spatial structure quantified in the logarithm space. For a stationary random function $V(x)$, the variogram $\gamma_V(h)$ and the covariance $C_V(h)$ at a distance lag h are linked in the following way:

$$\gamma_V(h) = \sigma^2_V - C_V(h) \quad (8)$$

where σ_V is the standard deviation of V. From Eq (8), the covariance of $Y(x)$, with $Y(x) = \ln[V(x)]$, can be estimated from γ_Y at each distance lag h. The next step consists in calculating the covariance of $V(x)$ from C_Y estimates using Eq (3). Finally, γ_V is derived from C_V estimates for each distance lag h.

3 SPATIAL STRUCTURE

In the following, the average isotropic variogram for each rainfall group and each quantity of interest is estimated. As the network consists of 16 sampling location, 120 pairs of points are available at each time step.

3.1 Averaged spatial structure

Isotropic variograms of the different quantities of interest (N_t, D_m and R) have been estimated for the different types of rainfall (convective, transitional and frontal). Figure 1 presents the sample variogram of N_t for each rainfall type at a 60-s temporal resolution. It is clear that the network is not extended enough to catch the *range* of the variogram (corresponding to the decorrelation distance). But it also clearly shows that there is a spatial structure in the DSD field (i.e., that the field is organized and not randomly varying) even at such a small scale (interdistances below 800 m). In terms of rainfall types, the variability observed over the monitored area is larger for convective events than for transitional and for frontal ones. For example, for an interdistance of about h =225 m, the variogram value is about 2384.5, 1181.5 and 787.8 m^{-6} for convective, transitional and frontal type rain events respectively at a 60-s temporal resolution. This corresponds to an

average difference of about 48.8, 34.4 and 28 drops per m^{-3} between two locations 225 m away.

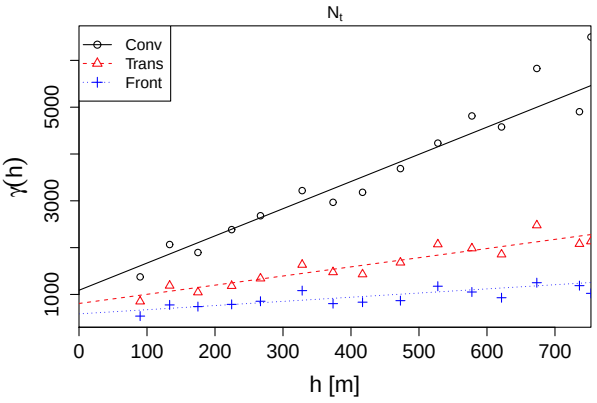

Figure 1: Sample variogram and fitted linear variogram model for N_t for the three rainfall types at a 60-s temporal resolution. The units associated with $\gamma(h)$ are m^{-6}. The X axis shows the interdistance classes (m).

To ease the comparison between rainfall events of different types, a variogram model was fitted on each empiral variogram. Because the range is not reached at the scale of the network, a linear variogram model is used. The high coefficients of determination (R^2) confirm the goodness of fit of this linear model to the experimental variogram values. For instance, R^2 is about 0.91, 0.90 and 0.74 for rain rate at a 60-s temporal resolution for convective, transitional and frontal rain events respectively. The linear models are considered valid up to 800 m and the authors recommend to not extrapolate these models at much larger interdistance classes. It has to be noticed that variogram models have been adjusted using the *gstat* package (Pebesma, 2004). Each linear model is characterized by two parameters: the *nugget* and the *slope*. The *slope* parameter indicates how fast is varying $Z(x)$ with the distance lag. The *nugget* quantifies the variability at very short distance lags (with respect to the minimum distance lag of the network). The nugget effect is explained by the possible variability of the considered process at interdistances smaller than the minimum interdistance in the network (all micro-scale variability, below 80 m in our case) and/or measurement errors. The linear model fitted on each sample variogram is also plotted in Figure 1. Figures 2 and 3 show the same information for D_m and R.

Figures 1-3 show that there is a spatial structure at this scale for all the quantities of interest. Moreover and as intuitively expected, the nugget and slope parameters are increasing from frontal to

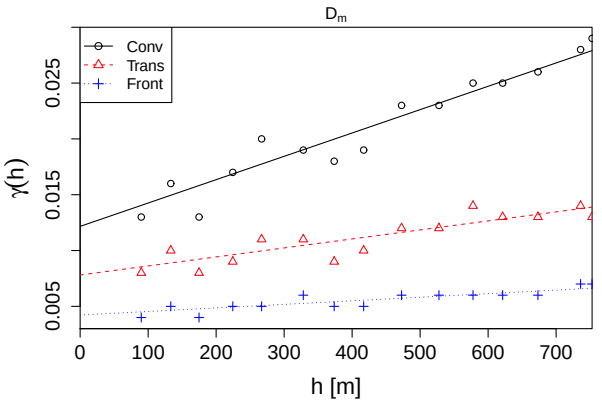

Figure 2: Same as Figure 1 for D_m. The units associated with $\gamma(h)$ are mm^2.

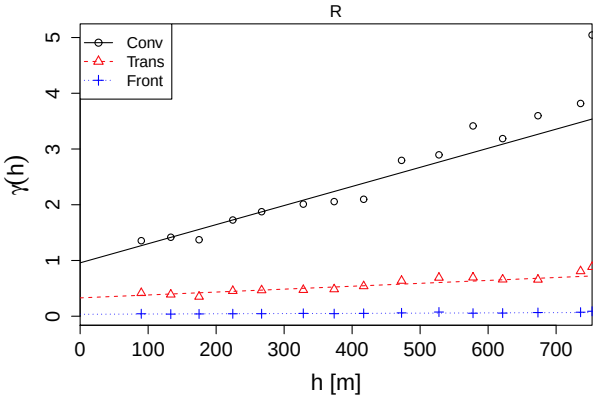

Figure 3: Same as Figure 1 for R. The units associated with $\gamma(h)$ are $mm^2\ h^{-2}$.

transitional to convective events. For instance, for N_t, the nugget (slope) of the transitional and frontal group represents about 74% (34%) and 54% (15%) of the one estimated for the convective group. These percentages for D_m exhibits similar values while the differences between convective and frontal parameters for R are larger. For example, the nugget (slope) parameter for frontal events represents about 4% (1%) the one for convective events. The nugget explains a larger part of the total variability (interpreted as a stronger influence of the measurement error) for frontal than for transitional and convective events.

3.2 Influence of the temporal resolution

The variogram has been estimated and a linear model has been fitted at 7 temporal resolutions ranging from 60 s to 1 h. For illustration, the evolution of the fitted nugget and slope values is presented in Figures 4 for N_t. Independently of the quantity of

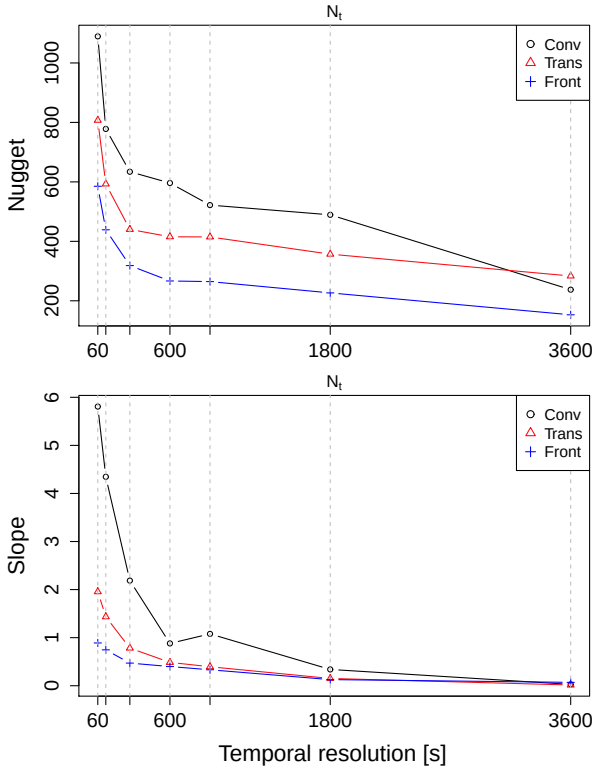

Figure 4: Influence of the temporal resolution on the nugget (top) and slope (bottom) parameters of the linear variogram model for the different types of rainfall.

interest, there is a strong decrease in the nugget and slope values until a temporal resolution of 600 s, followed by a much more limited decrease. The slope of the variogram decreases with decreasing temporal resolution until it reaches zero (or very close to zero) at temporal resolution of 30 min independently of the type of rainfall. This shows that for large temporal resolutions, i.e., 30 min and above, the sample variogram is basically flat and the fitted variogram model is a pure nugget model (slope$\sim$0) which indicates that the natural variability of the DSD (if any) is below the noise level in the observations. In other words, the integration in time of the DSD measurements tends to remove the variability existing at high temporal resolution, and the remaining (limited) variability is solely due to measurement errors.

4 CONCLUSION

A network of 16 disdrometers has been deployed over a typical weather radar pixel in Lausanne, Switzerland. A selection of 36 rainfall events, classified according to their type (convective, frontal, transitional), is considered in the present analysis. A geostatistical approach is considered in order to quantify the spatial structure of the raindrop size distribution (DSD). Isotropic variograms have been calculated foreach type fo rainfall for N_t, D_m and R. Overall, it shows that there is a spatial structure of the DSD, i.e., the fields are organized and not randomly distributed, even at 1 km^2 scale. Moreover, the experimental variograms highlight that the range (or decorrelation distance) is not reached at the scale of the network. Consequently a linear variogram model is fitted on each experimental variogram and is considered as valid at least at the scale of the network.

The temporal resolution has a strong impact on the evolution of the nugget and the slope of the linear models. It shows that for increasing time steps, the observed variability is decreasing. At a temporal resolution of 30min and above, the observed variability is mainly dominated by the measurement errors.

To illustrate possible applications of these results, it is possible to quantify the error associated when using point measurements extended at the pixel scale (and vice-versa). Moreover, the influence of the observed variability of the DSD on radar power laws and radar rain-rate estimations can be quantified (see for instance poster P.135: "*Influence of the small-scale variability of the raindrop size distribution on radar power laws.*").

Acknowledgments. This research is supported by the Swiss National Science Foundation (grant 200020-132002).

REFERENCES

Armstrong, M. and P. Delfiner, 1980: Towards a more robust variogram: A case study on coal. Technical Report N-671, Centre de Géostatistique, Fontainebleau, France.

Chilès, J.-P. and P. Delfiner, 1999: *Geostatistics: Modeling spatial uncertainty*. Probability and statistics, Wiley, 695 pp.

Jaffrain, J. and A. Berne, 2011: Experimental quantification of the sampling uncertainty associated with measurements from Parsivel disdrometers. *J. Hydrometeor.*, **12**, doi:10.1175/2010JHM1244.1.

Jaffrain, J., A. Studzinski, and A. Berne, 2011: A network of disdrometers to quantify the small-scale variability of the raindrop size distribution. *Water Resour. Res.*, **47**, doi:10.1029/2010WR009872.

Kruger, A. and W. F. Krajewski, 2002: Two-dimensional video disdrometer: a description. *J. Atmos. Oceanic Technol.*, **19**, 602–617.

Lee, C. K., G. Lee, I. Zawadzki, and K. Kim, 2009: A preliminary analysis of spatial variability of raindrop size distributions during stratiform rain events. *J. Appl. Meteor. Climate*, **48**, 270–283, doi:10.1175/2008JAMC1877.1.

Matheron, G., 1965: *Les variables régionalisées et leur estimation*. Masson et Cie, Paris, 305 pp.

Pebesma, E. J., 2004: Multivariate geostatistics in S: the gstat package. *Comput. Geosci.*, **30**, 683–691, doi:10.1016/j.cageo.2004.03.012.

Tapiador, F. J., R. Checa, and M. De Castro, 2010: An experiment to measure the spatial variability of rain drop size distribution using sixteen laser disdrometers. *Geophys. Res. Lett.*, **37**, doi:10.1029/2010GL044120.

Tokay, A. and P. G. Bashor, 2010: An experimental study of small-scale variability of raindrop size distribution. *J. Appl. Meteor. Climate*, **49**, 2348–2365, doi:10.1175/2010JAMC2269.1.